Check for updates

Tough polycyclooctene nanoporous membranes from etchable block copolymers†

Brenden D. Hoehn, [a] Elizabeth A. Kellstedt [b] and Marc A. Hillmyer ⋆[b]

Porous materials with pore dimensions of the nanometer length scale are useful as nanoporous membranes. ABA triblock copolymers are convenient precursors to such nanoporous materials if the end blocks are easily degradable (*e.g.*, polylactide or PLA), leaving nanoporous polymeric membranes (NPMs) if in thin film form. The membrane properties are dependent on midblock monomer structure, triblock copolymer composition, overall molar mass, and polymer processing conditions. Polycyclooctene (PCOE) NPMs were prepared using this method, with tunable pore sizes on the order of tens of nanometers. Solvent casting was shown to eliminate film defects and allowed achievement of superior mechanical properties over melt processing techniques, and PCOE NPMs were found to be very tough, a major advance over previously reported NPMs. Oxygen plasma etching was used to remove the surface skin layer to obtain membranes with higher surface porosity, membrane hydrophilicity, and flux of both air and water. This is a straightforward method to reliably produce highly tough NPMs with high levels of porosity and hydrophilic surface properties.

Introduction

Nanoporous polymeric membranes (NPMs) are materials that have pore dimensions on the nanometer or sub-nanometer length scale. Such exceptionally small pores allow these materials to be used for a variety of interesting applications. NPMs are commonly used in water treatment processes, such as ultrafiltration, where contaminants (*e.g.*, microbes, organic matter, natural macromolecules) are selectively rejected from the nanoscopic pores based on their hydrodynamic size.[1] Additionally, NPMs could be used for other public health applications, such as highly selective air filters that could be useful for the elimination of airborne contaminants. NPMs are also used as separators in lithium-ion batteries because they allow ion flux through the membrane while insulating the two electrodes.[2,3] Furthermore, NPMs are becoming more widely used for biomedical applications, including drug delivery, immunoselection, and biosensing.[4,5] Recently, nanoporous membranes have been used to produce nanometer-scale bubbles (nanobubbles) by passing high-pressure gas through the membrane into a liquid medium, and this technology could have promising applications in the field of blood oxygenation and treatment of hypoxia.[6–8]

For a membrane to successfully be optimized for an intended application, it must have a narrow pore size distribution to provide it with high selectivity, high void fractions to provide the membrane with high permeability, tunable pore sizes, and requisite mechanical robustness. There are several common methods used to fabricate NPMs. One method which produces NPMs with very narrow pore size distributions is track etching, where polymer films are bombarded with high-energy particles to produce pores or tracks that are subsequently etched to widen.[9] While the selectivity of these membranes is high, there is often a selectivity-permeability tradeoff due to low levels of porosity.[10] Another method is nonsolvent induced phase separation (NIPS), where membrane fabrication is performed by exposing a concentrated homopolymer solution to a nonsolvent for the polymer. The influx of nonsolvent causes the solution to demix into polymer-rich and polymer-poor domains, which become the membrane matrix and pores respectively.[11] While NIPS can produce high porosity membranes, it typically leads to stochastic pore size distributions, greatly reducing selectivity. An ideal membrane has both high selectivity (narrow pore distribution) and high porosity (pore density).[1]

Block copolymers are composed of two or more distinct macromolecules covalently bonded together, and the incompatibility of these components leads to microphase separation.[12] This feature offers a unique opportunity for nanoporosity because the domain spacing between phase-separated blocks is on

[a] Department of Chemical Engineering and Materials Science, University of Minnesota, Minneapolis, MN 55455-0431, USA

[b] Department of Chemistry, University of Minnesota, Minneapolis, MN 55455-0431, USA. E-mail: hillmyer@umn.edu

† Electronic supplementary information (ESI) available: The accompanying ESI is available which includes materials, synthetic methods, and characterization (NMR and FT-IR spectra, DSC traces, WAXS, tensile testing data, and additional SEM micrographs). See DOI: https://doi.org/10.1039/d3sm01498c

the order of tens of nanometers.[12,13] ABA triblock copolymers are convenient precursors to nanoporous materials if the end blocks are easily degradable (*e.g.*, polylactide or PLA), leaving nanoporous polymeric membranes (NPMs) if in thin film form. Processing triblock copolymers into the desired shape (*e.g.*, thin films) and then selectively degrading one of the blocks creates membranes with high void fractions and pore sizes of tens of nanometers. Thus, etching block copolymers is a promising method to produce nanoporous membranes with both narrow pore size distributions and high permeabilities.[1,14]

Etchable block copolymers are also highly tunable, allowing pore sizes to be tuned by changing the copolymer composition. Increasing pore dimensions is possible by increasing the degree of polymerization (N) or the volume fraction of the etchable block (f_A). Furthermore, modifying these two parameters in a block polymer system can result in several different self-assembled equilibrium morphologies. Diblock and triblock copolymers that self-assemble into hexagonally packed cylinders are commonly used for nanoporous membranes, where the cylinders are composed of the etchable block and become cylindrical pores.[15] Ideally, the cylinders are aligned perpendicular to the membrane surface to effectively allow the fluid flux; however, this requires careful surface energy control to obtain alignment.[16] The gyroid phase has been used for ultrafiltration membranes and does not require any additional alignment steps; however, the use of this phase in membrane applications is not common because it can be difficult to access the narrow gyroid phase space and the tunability of pore sizes is limited.[17] The use of a microphase separated state that lacks long-range order (disordered bicontinuous morphology) offers advantages over both equilibrium morphologies (cylindrical and gyroid) because there is no need for pore alignment, high porosities are achievable, and there is a wide range of block copolymer compositions that can be utilized to tune pore sizes.

Linear polylactide-*block*-polyethylene-*block*-polylactide (PLA-*b*-PE-*b*-PLA, abbreviated LEL) triblock copolymers are a suitable polymer system to access the disordered bicontinuous state for NPM development, where the high degree of chemical incompatibility between blocks leads to a microphase separation between PE and PLA blocks, and the high dispersity ($Đ$) and/or the high degree of entanglement in the PE domains prevent the adoption of equilibrium morphologies, resulting in a disordered bicontinuous morphology.[18–22] The PLA blocks are etched by immersing LEL films in an NaOH solution to produce NPMs with pore dimensions on the order of tens of nanometers. There are several advantages of using disordered bicontinuous PE-based nanoporous membranes over alternative materials. Aside from the small pore sizes and narrow pore size distribution, PE intrinsically has a high chemical resistance and melting temperature (T_m = 130 °C), giving membranes high thermal and chemical stability once produced. However, there are also disadvantages to using PE as a membrane material through etching of LEL precursors. For instance, melt processing is difficult due to the high melting temperature and high viscosity, making it difficult to obtain defect-free films. Solution processing is also difficult due to the low solubility at room temperature. Successful solution casting requires dissolving the triblock in tetralin at 140 °C, then pouring it into an aluminum pan placed on a hot plate (140 °C) to allow the solvent to evaporate.[18] It is not possible to remove the polymer from the pan without damaging the film, so the aluminum pan must be dissolved in 4 M HCl before the membrane can be etched with NaOH. Therefore, research into alternatives to PE and developing milder processing methods to develop NPMs from etchable block copolymers is desirable.

The PE polymer precursor in the LEL synthesis, polycyclooctene (PCOE), has a lower melting temperature (T_m = 54 °C) and is much more soluble at room temperature, greatly improving membrane processing conditions. Additionally, the alkene group in the backbone of PCOE can serve as a functionalization site to tune the membrane surface chemistry and provides the membrane with higher durability. In this study we report the synthesis and processing of polylactide-*block*-polycyclooctene-*block*-polylactide (PLA-*b*-PCOE-*b*-PLA, abbreviated LCL) triblock copolymers to obtain highly tough PCOE NPMs with tunable pore sizes, high porosities, hydrophilic surface properties, and enhanced permeabilities.

Experimental

Polymer synthesis

A 16-carbon diol (C_{16}-diol) CTA has recently been reported to effectively mediate chain transfer during the ring-opening metathesis polymerization (ROMP) of cyclooctene with high degrees of end-group functionality and control over molar masses.[23] Following this procedure, the CTA was synthesized by reducing ω-7-hexadecenlactone to *cis*-7-hexadecene-1,16-diol using lithium aluminum hydride (additional experimental details can be found in ESI†). Hydroxy telechelic PCOE was synthesized using the following procedure (Scheme 1). Distilled *cis*-cyclooctene (5.0 g, 45.4 mmol) and C_{16}-diol CTA (26.2 mg, 0.10 mmol) were added to a roundbottom flask to make a 2 M solution using distilled 2-methyltetrahydrofuran (2-MeTHF, 20 g, 232 mmol). Later, the solvent was changed to anhydrous toluene to avoid the risk of peroxide formation associated with 2-MeTHF, with no observable differences in polymer molar mass or dispersity. After sparging with argon gas for 20 minutes at room temperature, the solution was heated to 40 °C and Grubbs 2nd generation catalyst (G2, 0.77 mg, 0.0009 mmol) was added *via* syringe in a 1 mL stock solution (0.002 mol%, 0.015 wt%, 154 ppm G2 relative to COE, 18 ppm ruthenium relative to COE). Within two minutes of the addition of the catalyst, stirring ceased because of the increase in viscosity. After 30 minutes, the reaction was terminated by quenching the catalyst with ethyl vinyl ether, and the polymer was purified through precipitation in methanol.

The terminal hydroxyl groups on hydroxy-telechelic PCOE can initiate the ring-opening transesterification polymerization (ROTEP) of lactide to form LCL triblock copolymers.[24] The use of D,L-lactide is preferred over L-lactide because D,L-lactide
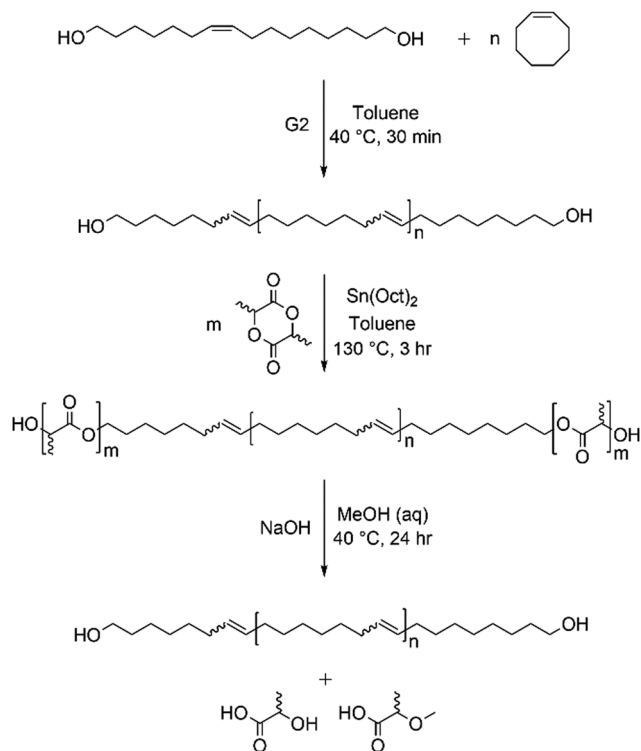
Scheme 1 Synthesis of Hydroxy Telechelic PCOE and LCL Triblock Copolymers followed by degradation of PLA to form nanoporous PCOE.

produces atactic PLA, whereas using L-lactide would result in a stereoregular PLA block. Semicrystalline PLA is undesirable because it introduces an additional thermal transition and has the potential to disrupt phase separation through breakout crystallization.[25,26] Additionally, amorphous PLA is more easily hydrolyzed in the etching process.[27] A standard LCL triblock polymerization was performed by adding PCOE (1.5 g, approx. 0.03 mmol) and D,L-lactide (1.8 g, 12.4 mmol) to a pressure vessel in a dry glove box. Tin(II) 2-ethylhexanoate (Sn(Oct)$_2$) catalyst (4.6 mg, 0.011 mmol) was delivered in a 1.0 mL stock solution of toluene (0.1 mol%, 0.3 wt%, 2600 ppm Sn(oct)$_2$ relative to D,L-lactide, 760 ppm Sn relative to D,L-lactide). The pressure vessel was then sealed, taken out of the glove box, and heated to 130 °C while stirring for three hours. The reaction was terminated by precipitating the LCL triblock copolymer twice in methanol and drying at 40 °C *in vacuo* to yield a fine polymer powder. Modifying the mass ratio of lactide:PCOE allows for various PLA volume fractions to be targeted.

Polymer processing

Triblock copolymers were processed into films using two different methods. Melt processing (thermocompression) was used to form triblock copolymers into thin films (approximately 300 μm) using a hydraulic melt press. To ensure thorough melting, the platen temperature was set to 100 °C. The polymer powder (300–500 mg) was placed between two Kapton films, which were further sandwiched between two metal panels. This was placed in between the two heating plates for five minutes without applying pressure to allow the polymer to soften. After the polymer had melted, the polymer was pressed with 8900 Newtons (2000 lbs, approximately 6 MPa) of force over a polymer area of 10–20 cm^2 for five minutes. After pressing, the steel panels and polymer were transferred to a water-cooled heat sink to cool the polymer, allowing the temperature to decrease by approximately 80 degrees in less than 2 minutes.

Solvent casting was also used to form triblock copolymers into thin films (approximately 100 μm). The triblock copolymer was dissolved in chloroform to make a 3.2 wt% polymer solution (50 mg polymer per mL solvent). After the polymer completely dissolved, the solution was passed through a 0.4 μm PTFE syringe filter. The solution was placed in a vial on the benchtop for 10 minutes to degas and remove air bubbles. The solution (5 mL) was gently poured into a PTFE evaporating dish (6 cm diameter) and placed in a desiccator with a cracked lid to shield the evaporation process from circulating air currents within the laboratory. The solutions were left for at least 12 hours to allow the chloroform to evaporate. The PTFE dishes were then moved into an oven at 40 °C for 45 minutes, followed by 12 hours of drying at 40 °C *in vacuo*. LCL films were then placed in an oven at 70 °C to anneal above the melting temperature of the samples. After 20 minutes, they were removed from the oven and placed on a benchtop to cool.

After processing into films, the PLA blocks of the triblock were etched to form nanoporous membranes. The following conditions were found to be effective for etching PLA from LCL triblock copolymers. A 0.5 M NaOH solution was made in a 70/30 v/v mixture of methanol and water. The melt-processed film was submerged in the alkaline solution and placed in an oven at 40 °C for 24 hours to completely hydrolyze the PLA block, leaving a nanoporous PCOE membrane. The membrane was then immersed in a 70/30 v/v solution of methanol twice, and 100% methanol twice (one hour per immersion step) to ensure full removal of NaOH from the membrane. Finally, the membrane was placed under dynamic vacuum at room temperature to remove residual methanol.

Plasma etching is a surface cleaning treatment that removes the top layer of a surface through ablation.[28] Oxygen plasma etching was performed using a PDC-001-HP (115 V) high power expanded plasma cleaner coupled with a Plasmaflo PDC-FMG gas regulator (Harrick Plasma). Nanoporous PCOE membranes were placed on the quartz sample tray followed by chamber evacuation. After the pressure reached ≤200 mTorr the oxygen valve was opened while the vacuum remained on. The system was allowed to equilibrate for 3–5 minutes to achieve a chamber pressure of 400–700 mTorr and oxygen flow rate of 8 mL min^{-1}. Plasma was produced by supplying the radiofrequency (RF) coil with 30 Watts of power at 8–12 MHz to produce oxygen plasma. Exposure times varied from 5 seconds to 10 minutes. After the specified exposure time, power was removed from the RF coil, and the oxygen was allowed to continue flowing for 10 seconds. The oxygen valve was closed allowing the chamber pressure to decrease below 200 mTorr. Finally, the vacuum was turned off and the chamber was slowly vented to atmospheric pressure.

Polymer characterization

Monomer conversion was determined using proton nuclear magnetic resonance (^{1}H NMR) spectroscopy, where the integration of unreacted COE (m, δ = 5.55 ppm) was compared to the alkene signal present in each repeat unit (m, δ = 5.40 ppm). Assuming two hydroxyl groups per chain, end-group analysis was performed on purified PCOE samples to determine the number average molar mass (M_n). To identify samples, the M_n in kg mol^{-1} is included in brackets after the name (e.g., PCOE [49] has an M_n of 49 kg mol^{-1}). The integration of the protons on the methylene groups adjacent to terminal hydroxyl groups (q, δ = 3.66 ppm) were compared to the alkene signal in the repeat unit.

The lactide conversion percentage was determined by comparing the integration of the PLA block methine proton (m, δ = 5.10–5.25 ppm) to residual D,L-lactide (q, δ = 4.77 ppm). The mass fraction of the PLA block (w_{PLA}) was determined by comparing the integration of the PCOE alkene protons to the PLA methine proton. Notation for triblock copolymer samples includes the molar mass of each block in kg mol^{-1} in brackets (e.g., LCL [24-49-24] comprises PLA end blocks of 24 kg mol^{-1} and a PCOE midblock of 49 kg mol^{-1}). The total molar mass of the triblock copolymer is determined by summing the molar masses of the end and midblocks. The volume fractions of each block (f_{PLA} and f_{PCOE}) are determined by dividing each mass fraction by its respective block density. In theory, these two values sum to 1, but slight deviations can occur from error in ^{1}H NMR integrations and density values. Therefore, the volume fractions reported in Table 1 have been normalized by the sum of each block contribution $\left(\frac{w_{PLA}}{\rho_{PLA}} + \frac{w_{PCOE}}{\rho_{PCOE}}\right)$ using previously reported density values for PCOE and PLA (ρ_{PCOE} = 0.88 g cm^{-3}, ρ_{PLA} = 1.25 g cm^{-3}).[29–31]

Size exclusion chromatography (SEC) with tetrahydrofuran (THF) as eluent was used to determine the molar mass distributions, $Đ$, and weight average molar mass (M_w). $Đ$ was determined using refractive index detection and M_w was determined using light scattering. Previous studies report that the dn/dc values for hydroxyl telechelic PCOE and PLA in THF are 0.11 mL g^{-1} and 0.049 mL g^{-1} respectively.[32,38] Weighted average dn/dc values were calculated for the LCL triblock copolymers, approximately 0.08 mL g^{-1} for all triblock copolymers in this study.[33]

Differential scanning calorimetry (DSC) was used to analyze the thermal behavior of both PCOE and LCL polymer samples. DSC data were acquired using heating and cooling rates of 10 °C min^{-1}. Small-angle X-ray scattering (SAXS) to determine the morphology of the LCL triblock copolymer and nanoporous PCOE. Samples were sealed in DSC pans under nitrogen. A variable temperature SAXS analysis of a solvent cast, non-annealed LCL film was performed by taking an initial measurement at 25 °C, then heating the sample to 80 °C and annealing for 20 min. The sample was then cooled to 40 °C and allowed to anneal for 30 min before cooling back to 25 °C. A room-temperature SAXS analysis of nanoporous PCOE was also performed.

PLA-etched membranes were analyzed using scanning electron microscopy (SEM). Surface images were obtained by mounting membranes flat on the sample stage. Samples were prepared for cross-sectional imaging by immersing methanol-infused membranes in liquid nitrogen for 3 minutes, fracturing the membrane, drying under vacuum, and mounting vertically on the sample stage. All samples were sputter coated with 2 nm of platinum to avoid charge buildup. Nominal pore diameters were determined using ImageJ software to manually measure pores from cryo-fractured membranes, with 4 nm added to reported values to account for platinum deposition. The measurement of circular-shaped pores was relatively straightforward, where the diameter of each pore was determined by measuring the distance between individual PCOE features. For pores with more complex geometries (i.e., ovals, horseshoes, etc.) the pore diameter was taken to be the length of the minor axis, which is perpendicular to the longest pore feature.

Uniaxial tensile testing was performed to determine the stress–strain behavior and the toughness of the membranes. Triblock films were prepared from LCL [25-51-25] by melt

Table 1 PCOE and LCL characterization

Polymer ID	% Conversion[a]	$M_{n,PCOE}$ (kg mol^{-1})[a]	$M_{n,PLA}$ (kg mol^{-1})[a]	$M_{n,LCL}$ (kg mol^{-1})[a]	M_w (kg mol^{-1})[b]	$Đ$[b]	w_{PLA}	f_{PLA}[c]	χN[d]	Nominal pore diameter[e]
PCOE [49]	99.9	49	—	—	73	1.9	0	0	—	—
PCOE [50]	99.9	50	—	—	67	1.8	0	0	—	—
PCOE [51]	99.9	51	—	—	71	1.8	0	0	—	—
PCOE [55]	99.9	55	—	—	80	1.9	0	0	—	—
PCOE [110]	99.9	110	—	—	105	1.9	0	0	—	—
LCL[24-55-24]	88.5	55	48	103	114	1.5	0.47	0.38	625	47 ± 13
LCL[26-55-26]	91.7	55	52	107	108	1.8	0.49	0.4	648	48 ± 23
LCL[25-51-25]	93.6	51	51	102	109	1.7	0.50	0.41	611	54 ± 14
LCL[26-50-26]	91.1	50	51	101	112	1.8	0.51	0.42	612	50 ± 14
LCL[25-49-25]	93.5	49	51	101	104	1.6	0.51	0.42	601	47 ± 14
LCL[49-110-49]	91.8	110	114	224	143	2.1	0.51	0.42	1153	110 ± 36
LCL[28-49-28]	94.3	49	57	106	105	1.7	0.53	0.44	630	64 ± 22

[a] ^{1}H NMR spectroscopy. [b] SEC using THF as the eluent at room temperature. M_w was directly measured using multi-angle light scattering while $Đ$ values were determined via refractive index. [c] Dividing mass fraction by the density of each block. [d] Estimating χN at 100 °C using solubility parameters with a reference volume of 118 Å^3. [e] Nominal pore diameter obtained from freeze-fractured SEM images with $n \geq 100$ pores measured.

pressing and solvent casting. After films were prepared, dog bone samples were prepared *via* die cutting and etched using the etching conditions described above. The tensile bars were 25 mm long, 3 mm wide in gauge region, and 0.1 mm thick. Tensile results are reported for $n \geq 5$ tensile bars tested.

Nitrogen sorption analysis was performed on a Quanta-chrome Autosorb iQ2, and data analysis was performed using ASiQwin software. Samples were degassed at room temperature for 24 hours prior to the analysis. Samples were then transferred to the analyzer and the pressure was isothermally raised to atmospheric pressure while monitoring the amount of nitrogen adsorbed (77 K), then slowly reduced once more (24 hours total), producing an isotherm. Surface area calculations were performed using the Brunauer–Emmett–Teller (BET) method in the linear regime of the isotherm, and pore size distributions were obtained using the Barrett–Joyner–Halenda (BJH) method (desorption isotherm). Contact angle measurements were performed by placing a single droplet (100 µL) of deionized water onto the membrane surface. A horizontal camera was used to obtain an image of the droplet and calculate the water contact angle. Water flux measurements were performed by placing pre-wet membranes in a cross-flow system with a flow rate of 300 mL min^{-1} at a pressure of 0.07 bar (10 psig). Gas flux measurements were performed by passing air through dry membranes at a pressure of 0.28 bar (4 psig). Flux results are reported as a mean followed by the range for $n \geq 3$ membranes in brackets (*i.e.*, mean [minimum–maximum]) in units of L m^{-2} h^{-1} bar^{-1}.

Results & discussion

Hydroxy telechelic PCOE was synthesized from COE *via* ROMP using a C$_{16}$-diol CTA. High monomer conversion percentages (99.9%) were routinely obtained. Molar masses were controlled by modifying the mole ratio of CTA to COE, and M_n was determined using end-group analysis. The hydroxyl end-groups initiated the ROTEP of D,L-lactide to synthesize LCL triblock copolymers with approximately 90% lactide conversion typically achieved. Various compositions of LCL triblock copolymers were synthesized by modifying the mass ratio of lactide to PCOE. ^{1}H NMR spectroscopy corroborated the formation of LCL triblock copolymers (Fig. S1 and S2, ESI†), as the proton signal adjacent to the PCOE end-groups shifted downfield from δ = 3.7 ppm (hydroxyl) to δ = 4.1 ppm (ester) after LCL triblock copolymer formation.[24] Representative SEC traces of a PCOE homopolymer and LCL triblock copolymer (Fig. 1) both show monomodal size distributions and dispersity values ranging from Đ = 1.5 to 2.1 (Table 1). The LCL triblock copolymer has a smaller elution time than the PCOE homopolymer, indicating a larger hydrodynamic volume and is further evidence that the lactide was incorporated into the triblock copolymer.

DSC was used to analyze the thermal behavior of LCL triblock copolymers (Fig. 2) and nanoporous PCOE (Fig. S7 and S8, ESI†). The melting temperature of LCL [26-50-26] was T_m = 54 °C, and the degree of crystallinity was 24%. Crystallinity
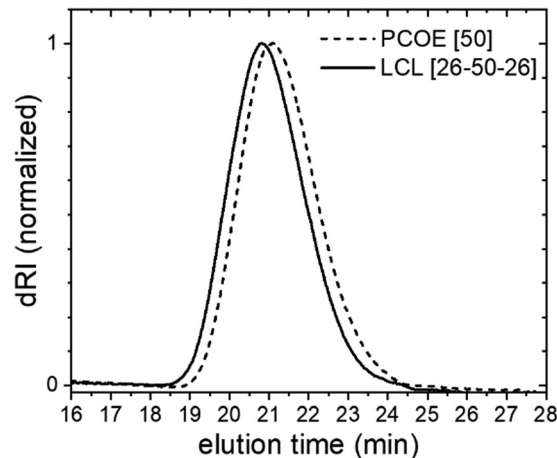

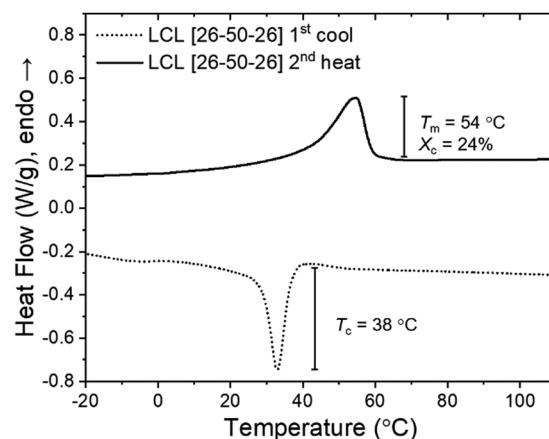Fig. 1 Representative SEC and of PCOE homopolymer and LCL triblock copolymer.

Fig. 2 DSC of LCL triblock copolymer after precipitation with a heating/cooling rate of 10 °C min^{-1}. Traces represent the first cool and second heat.

was determined by normalizing the enthalpy of melting from the 1st heating by the mass fraction of PCOE and that of 100% crystalline PCOE (230 J g^{-1}).[34] In both solvent cast and melt pressed membranes the melting temperature nanoporous PCOE was T_m = 61 °C, and the degree of crystallinity was approximately 32% (Fig. S7, ESI†). For comparison, poly-ethylene-based NPMs have typical melting temperatures of T_m = 130 °C and are about 60% crystalline. This lower melting temperature makes LCL melt processing more facile than LEL precursors to NPMs. Additionally, LCL is readily soluble in chloroform at room temperature, while LEL triblocks are only soluble in solvents above 100 °C. These characteristics make the development of PCOE NPMs more convenient than polyethylene NPMs.

Complete removal of PLA blocks is required to obtain functioning membrane materials. ^{1}H NMR spectroscopy was used to determine the full degradation of PLA by confirming the disappearance of the PLA methine and methyl peaks (Fig. S3, ESI†).

Furthermore, Fourier transform infrared (FT-IR) spectroscopy shows the absence of the carbonyl signal at 1750 cm^{-1} after PLA etching (Fig. S4, ESI†). The membrane porosity was examined and is consistent with the PLA volume fraction. Four different membranes derived from LCL [25-51-25] were gravimetrically analyzed before PLA etching, after PLA removal while infused with methanol, and after full methanol removal. Two different methods were used to determine the porosity of the samples. The first method was to determine the PLA mass fractions by normalizing the mass loss due to PLA etching by the initial film mass. This method yielded PLA mass fractions of w_{PLA} = 50.0 ± 0.2% and membrane porosities of 40.0 ± 0.2%, which are comparable to the PLA mass and volume fractions reported in Table 1. The second method was to determine the mass of infused methanol after PLA removal and compare the mass to the dried membrane; these masses were then converted to volume using a density conversion. The porosity was calculated by dividing the volume of infused methanol by the total volume of the membrane sample (dimensions measured using calipers). This method had more variability than the first, as it was difficult to ensure all methanol was wiped from the membrane surfaces without allowing mass loss from methanol evaporation. Nevertheless, the porosities obtained with this method were 38.8 ± 10.8%, corroborating PLA volume fractions are directly related to final membrane porosity.

While the PCOE domains in LCL triblock copolymers were 24% crystalline, PCOE NPMs were 31–32% crystalline, regardless of processing history (Fig. S7, ESI†). This increase in crystallinity suggests the PCOE domains undergo cold crystallization during the PLA etching process. To test this hypothesis, a membrane was etched at 21 °C then annealed at 40 °C for 3 hours; the membrane was 25% and 31% crystalline after each step (Fig. S8, ESI†), corroborating cold crystallization during the PLA etching process. Crystallinity helps stabilize pore structure at room temperature; accordingly, it is important not to subject the etched membrane to elevated temperatures to avoid melting-induced pore collapse.[18] Other studies have shown that membranes release surface energy during pore collapse as interfacial area decreases, resulting in an exothermic transition as measured using DSC.[35] For polystyrene membranes with similar surface areas, an exotherm of 3.5 J g^{-1} was observed while heating through the glass transition temperature as a result of pore collapse. Because pore collapse would similarly occur during heating through T_m in nanoporous PCOE, the energy released is likely obscured by the endothermic transition of melting (approximately 58 J g^{-1}). This may explain the apparent double peak in the DSC data for nanoporous PCOE (Fig. S7 and S8, ESI†).

Triblock copolymers were solvent cast and analyzed using SAXS to verify the morphology and to determine degree of long-range ordering. Variable temperature SAXS analysis of a solvent cast LCL [26-55-26] film shows the presence of a broad scattering peak with no higher order peaks is consistent with a disordered bicontinuous morphology (Fig. 3a) as confirmed in related LEL triblocks, where the triblock copolymer is microphase separated without long-range morphological order. Room temperature SAXS analysis was also performed on an
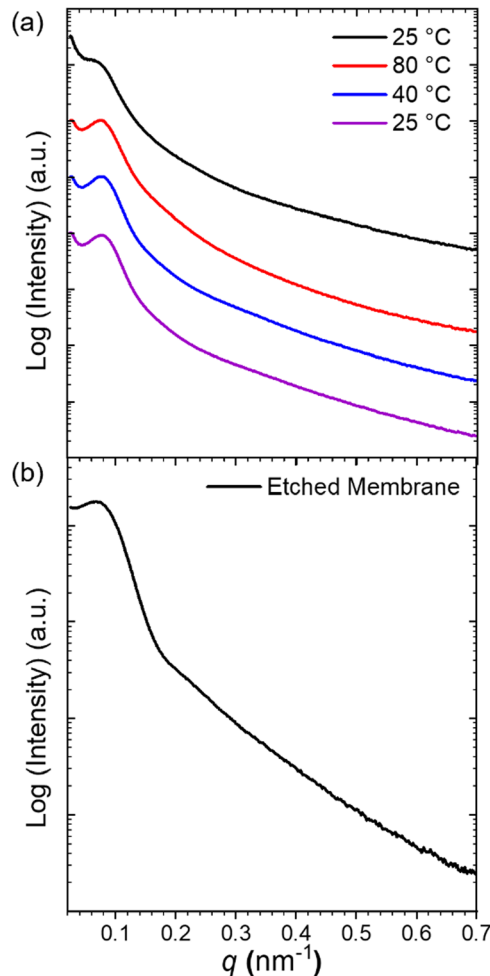

Fig. 3 (a) Variable temperature SAXS analysis of solvent cast LCL [26-55-26] triblock copolymer films. Curves correspond to 25 °C (black) as cast, 80 °C (red), 40 °C (blue), and 25 °C (purple) after thermal treatment. Samples were held isothermally at 80 °C for 20 minutes and 40 °C for 30 minutes. Shifted vertically for clarity. (b) Room temperature SAXS analysis of nanoporous PCOE derived from LCL [28-49-28].

etched membrane to confirm the original morphology remained after PLA was removed (Fig. 3b). The PLA–PCOE interaction parameter was estimated to be χ = 0.44 at 373 K, using previously reported solubility parameters: δ_{PLA} = 21.3 J$^{1/2}$ cm$^{-3/2}$ and δ_{PCOE} = 16.9 J$^{1/2}$ cm$^{-3/2}$.[36,37] The segregation strengths (χN) were estimated using these interaction parameters, and the volume normalized degree of polymerization was determined using a reference volume of 118 Å^3. The estimated segregation strengths of all LCL triblock copolymers prepared were over $(\chi N)_{LCL}$ = 600; therefore, these triblock copolymers have a strong thermodynamic drive to microphase separate and are all very strongly segregated. The absence of long-range ordering, and adoption of a disordered bicontinuous morphology, can be attributed to a high midblock dispersity and a high degree of entanglement in the PCOE blocks.[18,20–22,38] When the sample is heated above its melting temperature it maintains this morphology; however, the q-value of the primary scattering peak slightly increases as the sample is heated and annealed. This is associated with a decrease in real space domain spacing (d),

where d = 80 nm and d = 73 nm before and afterward heat treatment respectively. For comparison, the domain spacing for this system in a hexagonally packed cylindrical morphology is estimated to be about d = 100 nm, resulting in pore sizes approximately 66 nm in diameter.[39] While polymeric materials are known to thermally expand upon heating, we posit this system becomes denser upon heating because it was solvent cast. Since the solvent molecules continue to occupy space between polymer chains at the onset of crystallization, the polymer solidifies at a non-equilibrium density. When melted, polymer domains densify, leading to a decrease in domain spacing. Additionally, the intensity of the primary scattering peak appears to become more intense after melting (Fig. 3a), evidence that the sample becomes more strongly segregated.

Nanoporous membranes were also analyzed using SEM, where cross-sectional imaging revealed an interconnected and disorganized PCOE matrix (Fig. 4). Pore sizes were shown to be tunable by changing triblock composition. Pore sizes increased as both N and f_{PLA} increased. At a constant PLA volume fraction of f_{PLA} = 0.42, LCL [26-50-26] and LCL [49-95-49] produced NPMs with mean pore sizes approximately 50 nm and 110 nm respectively. Additionally, the mean pore sizes increased from approximately 50 nm to 64 nm when the PLA volume fraction was increased from f_{PLA} = 0.42 to f_{PLA} = 0.45. Since pore dimensions are directly related to the PLA molar mass, it is expected that membranes with pores smaller than 50 nm would be attainable. However, our approach here uses a disordered bicontinuous triblock morphology, and as molar mass decreases, self-assembly into ordered morphologies becomes more likely due to increased mobility at lower molar masses. For instance, we have shown that LCL [10-22-10] triblock copolymers form lamella microstructures

at similar PLA volume fractions and molar mass dispersities to those reported in this study.[38] Therefore, we expect this approach to NPM development to achieve pore diameters as small as 20 nm.

LCL [25-51-25] was used as a model polymer to determine the mechanical properties of NPMs fabricated under different processing conditions. The triblock copolymer was formed into films by melt pressing and solvent casting. The stress–strain behavior of both LCL films and respective NPMs were analyzed using tensile testing (Fig. 5). Solvent cast samples had superior mechanical properties than melt-pressed samples in both triblock and nanoporous form. The LCL triblock toughness was 101 ± 14 MJ m^{-3} and 36 ± 21 MJ m^{-3} for the solvent cast and melt-pressed samples, respectively. Similarly, the toughness was 33 ± 7 MJ m^{-3} and 0.3 ± 0.4 MJ m^{-3} for the NPMs from solvent cast and melt-pressed precursors, respectively. While convenient, melt processing can introduce both microscopic and macroscopic defects (*i.e.*, cracks, Fig. S10, ESI†) which localize stress and lower membrane toughness. Not only are cracks detrimental to the mechanical strength of a membrane, but they also reduce membrane selectivity in applications such as ultrafiltration or nanobubble generation. Solvent casting largely eliminates these film defects and leads to highly tough nanoporous membranes, making it the preferred processing
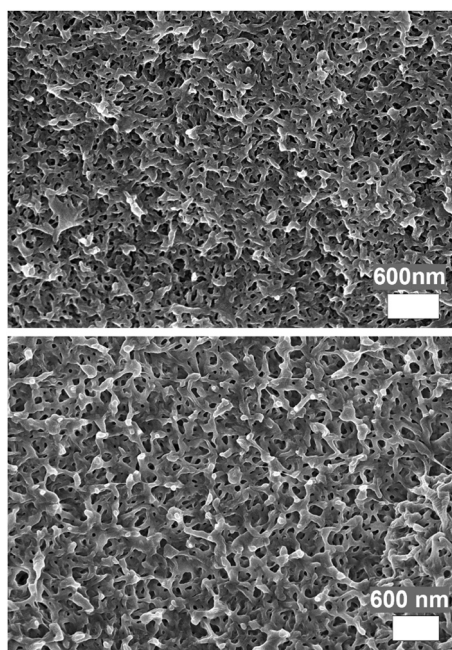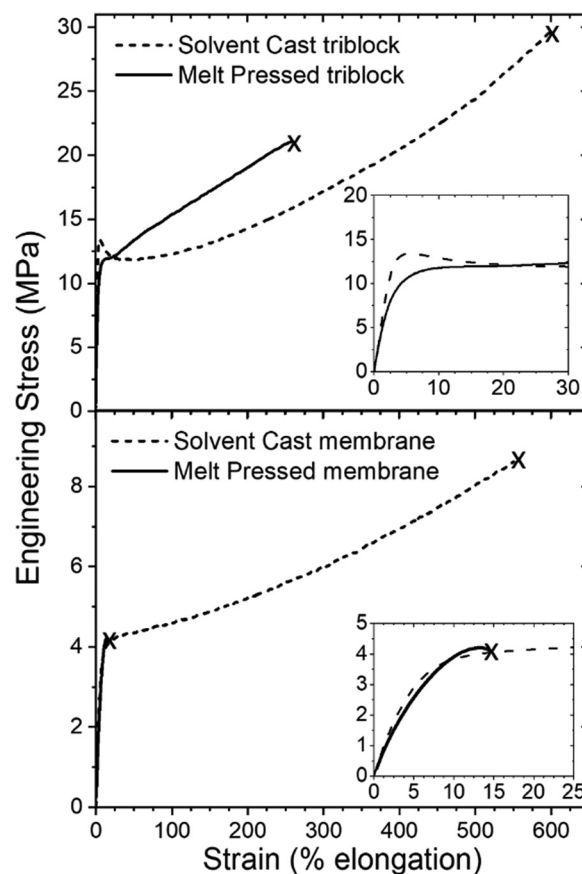

Fig. 4 Cross-sectional SEM images of cryo-fractured nanoporous PCOE membrane derived from (top) LCL [26-50-26] and (bottom) [49-95-49]. Samples coated with 2 nm platinum.

Fig. 5 Representative stress–strain curves from uniaxial tensile testing of LCL [25-51-25] triblock films (top) and nanoporous membranes (bottom) prepared by different processing methods. Insets: Low-strain regions enlarged for clarity.

method for PCOE-based NPMs. For comparison, the maximum toughness of three commercial membranes tested was 4 MJ m^{-3} (Table S2, ESI†), and the maximum toughness for the nanoporous polyethylene analog was 5 MJ m^{-3}.[18] While the alkene group in the PCOE backbone reduces crystallinity, providing the membrane with more durability compared to more highly crystalline polyethylene NPMs, PCOE can undergo oxidation upon aging (Fig. S6, ESI†), which can lead to membrane embrittlement.[40,41] Therefore, PCOE membranes should be stored under inert gas or reduced pressure to mitigate oxidation during long-term storage.

While solvent casting leads to enhanced mechanical properties, it also leads to the formation of an undesirable surface skin layer (Fig. 6a). This low-porosity skin layer is a result of differing block surface energies. It is thermodynamically unfavorable for a material to maintain a high surface energy. Since PCOE is a low surface energy polymer, PCOE preferentially aligns at the surface over PLA during solvent casting. This preference results in a dense PCOE layer on the top surface of the membrane, leading to low surface porosity (Fig. 6c). However, we note that this skin layer does not seem to significantly impact etching of PLA, evidenced by ^{1}H NMR spectroscopic analysis (Fig. S3, ESI†). This is likely because the bottom membrane surface does not form a skin layer (Fig. S11, ESI†), allowing PLA removal to begin at the bottom surface and progress through the film toward the top surface.

Plasma etching is a surface cleaning technique often used to clean or remove material surfaces, such as removing the skin of polymeric samples.[42–44] Oxygen plasma etching was performed on solvent cast membranes to remove the surface skin layer, and successful skin removal was completed by treating PCOE NPMs with 30 W of power supplied to the RF coil (Fig. 6b–d). At low plasma etching times (0–60 seconds), surface pore structure began to resemble cross-section pore structure (Fig. 4) and led to an increase in surface porosity, with 60 seconds leading to optimal surface pore structure. Under these conditions, the mean surface pore diameter measured was 57 ± 16 nm, within 6% of the cross-sectional pore diameter. However, at higher plasma etching times (120–600 seconds), surface pores began to increase in diameter and decrease in pore density. The most extreme plasma etching was conducted with 38 W of power for 600 seconds; this led to an entirely nonporous surface (Fig. S12, ESI†). The decrease in porosity and coarsening of pore sizes could be attributed to localized PCOE melting, leading to pore collapse and aggregation. Additionally, this could be a result of redeposition of material from the plasma etching process, where longer plasma times reduce the thickness of individual PCOE features while also re-depositing polymer fragments into existing pores.[45,46] Plasma etching the membranes does not lead to an appreciable decrease in mechanical strength (Table S1, ESI†).

Porous materials are often characterized using nitrogen sorption analysis, which allows for the surface area calculation using the BET method and the pore size distribution, using the BJH method.[47,48] Nitrogen sorption analysis was performed on LCL [25-51-25] membranes before and after plasma etching (Fig. 7). The resultant pore diameters were determined to be 34 nm for both samples, underestimating pore diameters compared to values obtained via SEM (54 nm). These membranes were found to have a narrow pore size distribution, with a full-width-half-max value of 9 nm before plasma etching and 11 nm after plasma etching. The corresponding surface areas for membranes before and after plasma etching were 46 and 48 m^2 g^{-1} respectively, suggesting the NPMs maintain their porosity after plasma etching. For comparison, if these membranes adopted a hexagonally packed cylindrical morphology, the expected surface area is estimated to be 88 m^2 g^{-1} (using 34 nm pores) and 55 m^2 g^{-1} (using 54 nm pores). While it is possible for pores to collapse after removal of PLA domains, the PCOE domains seem to have high enough crystallinity to support the nanoporous structure. However, the possibility of some degree of pore collapse cannot be completely ruled out, as the surface areas obtained by BET analysis are slightly lower than theoretical predictions based on a cylindrical morphology.
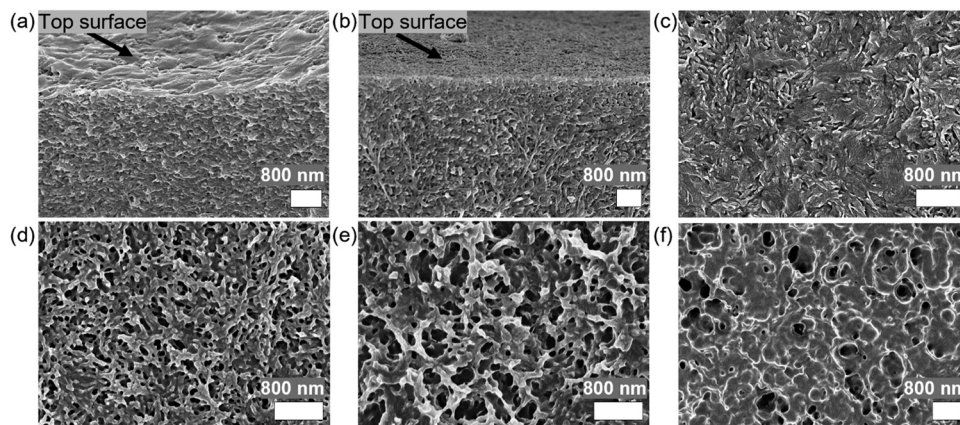

Fig. 6 (a) and (b) SEM images of cryo-fractured nanoporous PCOE membranes taken near the surface of membranes derived from LCL [25-51-25]. Both samples were solvent cast followed by annealing for 20 minutes at 70 °C prior to PLA etching. Additionally, sample (b) was plasma-etched for 60 seconds following PLA etching. (c)–(f) Surface SEM images of membranes plasma-etched for (c) 0 seconds, (d) 60 seconds, (e) 120 seconds, and (f) 600 seconds.
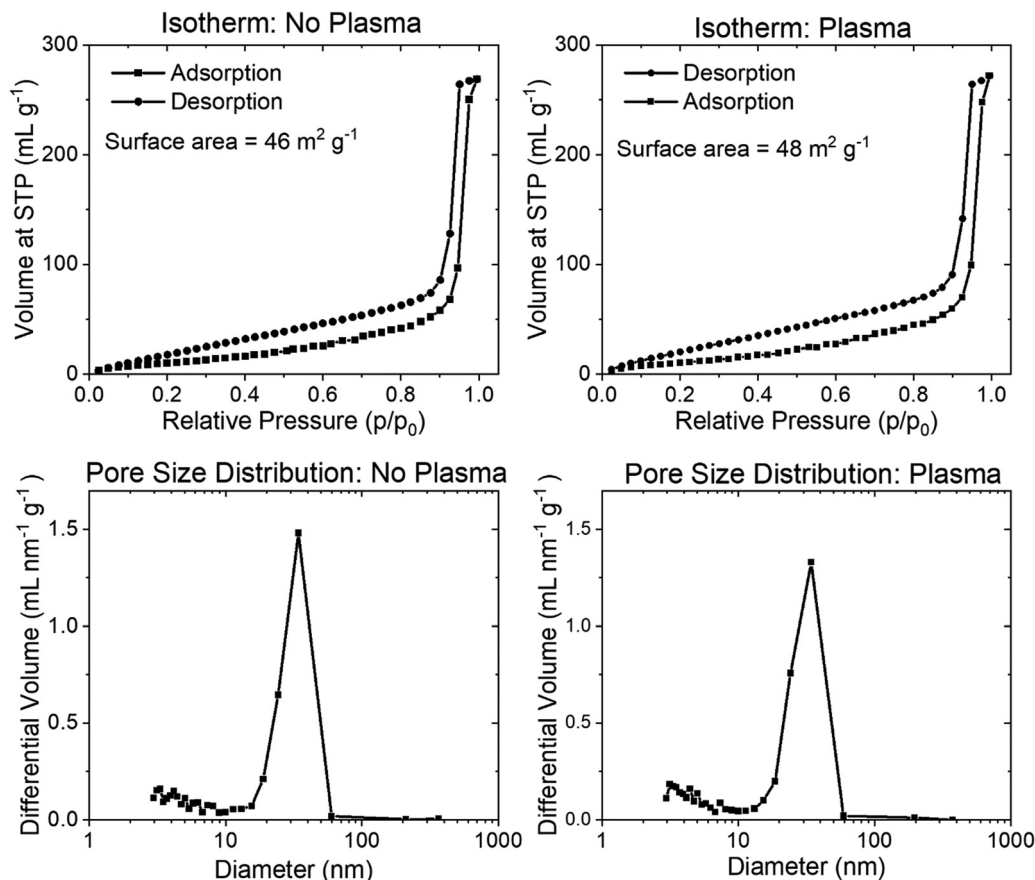
Fig. 7 Type IV Isotherms and corresponding pore size distributions from nitrogen adsorption analysis of PCOE membranes derived from LCL [25-51-25] before and after plasma etching. Surface area is determined using the BET equation and pore size distribution is determined using the BJH method. Mode pore diameters are calculated to be 34 nm in both samples.

Nevertheless, plasma etching PCOE NPMs is a fast and convenient way to remove the surface skin layer produced during solvent casting while maintaining membrane porosity.

Oxygen plasma etching also leads to a reduction in membrane hydrophobicity.[49] Non-plasma-etched PCOE NPMs have hydrophobic character, with a $107.7° \pm 1.5°$ water contact angle; while after plasma etching, the angle is reduced to $62.3° \pm 1.1°$ (Fig. 8a and b). The oxygen plasma consists of highly reactive oxygen radicals and ions which break carbon–carbon bonds and form carbon–oxygen bonds, leading to decreased hydrophobicity via incorporation of polar groups on the surface.[50] Membranes derived from LCL [25-51-25] were tested using a cross-flow filtration system to determine the flux of deionized water (Fig. 8c). Non-plasma-etched membranes had a water flux of 3.6 [3.2–3.9] L m^{-2} h^{-1} bar^{-1}, whereas the plasma-etched membrane flux was 7.6 [5.8–9.6] L m^{-2} h^{-1} bar^{-1}. In addition to ultrafiltration of water, these membranes could be used as air filters. To demonstrate, the volume of air that passed through the membrane was monitored to determine the gas flux. The gas flux for these membranes was 2180 [2050–2260] L m^{-2} h^{-1} bar^{-1} and 2890 [2400–3290] L m^{-2} h^{-1} bar^{-1} for non-plasma-etched and plasma-etched membranes respectively. The increase in air flux is attributed to skin layer

removal, while the increase in water flux is attributed to both skin layer removal and increased membrane hydrophilicity. The increased range in the plasma-etched flux measurements is likely a result of slightly different plasma etching conditions (*i.e.*, variations in plasma chamber pressure) or differences in the membrane thickness. The water permeability of the as-prepared PCOE membranes in this study is relatively low compared to alternative nanoporous membranes, and the reduced permeability is likely a combination of several factors such as the hydrophobic nature of the bulk of the membrane, the tortuosity, and large thickness of the selective layer (100 μm).[1,6,51] Whereas alternative membranes typically have lower tortuosities and much thinner selective layers (10s nm).

In addition to an increase in flux, plasma etching the membranes has an added benefit of exposing pores and reducing hydrophobicity on the membrane surface for a future application in nanobubble generation. Nanobubble size is directly related to surface pore size; therefore, obtaining control of surface pore size is necessary to obtain the desired size nanobubble.[52,53] This system could potentially be used for nanobubble generation because the membrane pore size is easily tunable by changing M_n or f_{PLA}; additionally, PCOE membranes are also highly tough and may not rupture as easily
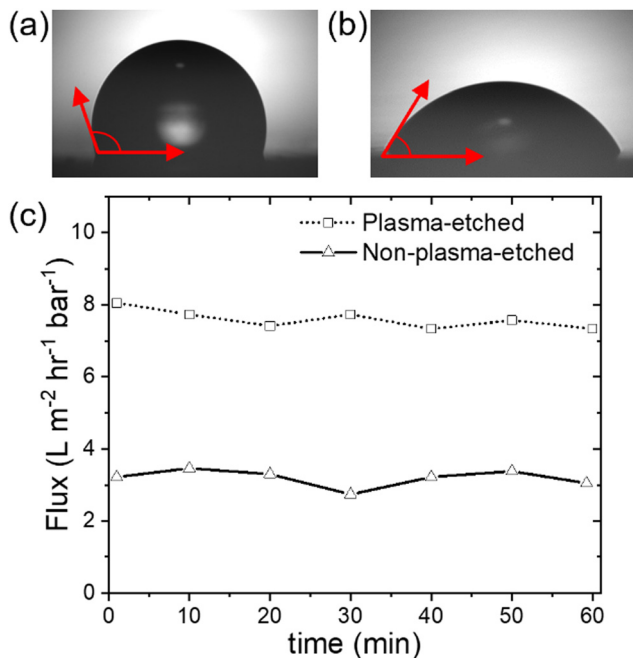
Fig. 8 Water contact angle measurements of (a) non-plasma-etched and (b) plasma-etched NPMs derived from LCL [25-51-25], and (c) representative water flux measurement.

as more brittle membranes. Plasma etching would be beneficial to nanobubble generation because it removes the skin layer and exposes pores, theoretically making nanobubble sizes tunable by changing the triblock composition without interference of a skin layer. The pressure required to form nanobubbles is proportional to the water contact angle, where lower water contact angles result in lower pressures needed to generate nanobubbles.[52] Moreover, the diameter of nanobubbles decreases with decreasing hydrophobicity.[54] Therefore, plasma-etched PCOE membranes could be successful in nanobubble generation, and additional surface modification techniques could be used to obtain more highly hydrophilic NPMs to generate nanobubbles.

Another potential application of these NPMs is ultrafiltration of water; however, fouling is a common issue in hydrophobic ultrafiltration membranes. One way to obtain fouling resistance is by reducing membrane hydrophobicity. The reduced hydrophobicity coupled with an increase in water flux make plasma etching PCOE NPMs a viable option to produce ultrafiltration membranes. Hydrophobicity can be further reduced in future studies. Oxygen plasma etching forms hydroxyl groups on membrane surfaces, which could be utilized to obtain fouling resistance by grafting hydrophilic moieties (e.g., polyethylene glycol) to the plasma-etched surface. Additionally, the backbone alkene could easily be functionalized with hydrophilic moieties through reactions such as thiol–ene click chemistry, an improvement over the relatively inert polyethylene NPMs previously reported.[18,55] Lastly, these membranes could be used as highly selective air filters during times of public health crisis.

Conclusion

Nanoporous PCOE membranes were developed by synthesizing LCL triblock copolymers, processing them into films, and then degrading the end blocks. Pore sizes were shown to be tunable by changing the overall molar mass of the triblock or the PLA volume fraction. These membranes were formed into thin films using both melt pressing and solvent casting techniques. Solvent casting produced membranes that had fewer defects and higher mechanical properties than melt pressing. In addition to milder processing conditions, nanoporous PCOE was also shown to have higher toughness than analogous PE membranes previously developed using similar strategies. Oxygen plasma etching was used to remove the surface skin layer to obtain membranes with high surface porosity and increased membrane hydrophilicity, along with higher air and water flux. Lastly, PCOE membranes can be functionalized in subsequent studies to tailor membranes for a particular application, giving these materials great potential for future ultrafiltration and nanobubble generation applications.

Author contributions

M. A. H. conceived of the project and designed the experimental approach in conjunction with B. D. H. Experiments were carried out by B. D. H. with assistance from E. A. K. for polymer synthesis and determining suitable PLA etching conditions. B. D. H. and M. A. H. contributed to data analysis and preparation of the manuscript.

Conflicts of interest

The authors declare no competing financial interest. The primary data underlying this study are openly available in The Data Repository for University of Minnesota (DRUM) at **https://doi.org/10.13020/xpma-vn76**.

Acknowledgements

References

1 N. Hampu, J. R. Werber, W. Y. Chan, E. C. Feinberg and M. A. Hillmyer, *ACS Nano*, 2020, **14**(12), 16446–16471.

2 P. T. Dirlam, R. S. Glass, K. Char and J. Pyun, *J. Polym. Sci., Part A: Polym. Chem.*, 2017, **55**(10), 1635–1668.

3 H. Yang, X. Shi, S. Chu, Z. Shao and Y. Wang, *Adv. Sci.*, 2021, **8**(7), 2003096.

4 S. P. Adiga, C. Jin, L. A. Curtiss, N. A. Monteiro-Riviere and R. J. Narayan, *Wiley Interdisc. Rev.: Nanomed. Nanobiotechnol.*, 2009, **1**(5), 568–581.

5 S. Y. Yang, J.-A. Yang, E.-S. Kim, G. Jeon, E. J. Oh, K. Y. Choi, S. K. Hahn and J. K. Kim, *ACS Nano*, 2010, **4**(7), 3817–3822.

6 M. Kukizaki and M. Goto, *J. Membr. Sci.*, 2006, **281**(1–2), 386–396.

7 T. Ma, Y. Kimura, H. Yamamoto, X. Feng, A. Hirano-Iwata and M. Niwano, *J. Phys. Chem. B*, 2020, **124**(24), 5067–5072.

8 R. Cavalli, A. Bisazza, P. Giustetto, A. Civra, D. Lembo, G. Trotta, C. Guiot and M. Trotta, *Int. J. Pharm.*, 2009, **381**(2), 160–165.

9 T. Ma, J.-M. Janot and S. Balme, *Small Methods*, 2020, **4**(9), 2000366.

10 A. Mehta and A. L. Zydney, *J. Membr. Sci.*, 2005, **249**(1–2), 245–249.

11 G. R. Guillen, Y. Pan, M. Li and E. M. V. Hoek, *Ind. Eng. Chem. Res.*, 2011, **50**(7), 3798–3817.

12 E. A. Jackson and M. A. Hillmyer, *ACS Nano*, 2010, **4**(7), 3548–3553.

13 W. Y. Chan and M. A. Hillmyer, *ACS Appl. Polym. Mater.*, 2022, **4**(11), 8009–8020.

14 T. Vidil, N. Hampu and M. A. Hillmyer, *ACS Cent. Sci.*, 2017, **3**(10), 1114–1120.

15 D. A. Olson, L. Chen and M. A. Hillmyer, *Chem. Mater.*, 2008, **20**(3), 869–890.

16 J. N. L. Albert, W.-S. Young, R. L. Lewis, T. D. Bogart, J. R. Smith and T. H. Epps, *ACS Nano*, 2012, **6**(1), 459–466.

17 L. Li, P. Szewczykowski, L. D. Clausen, K. M. Hansen, G. E. Jonsson and S. Ndoni, *J. Membr. Sci.*, 2011, **384**(1–2), 126–135.

18 L. M. Pitet, M. A. Amendt and M. A. Hillmyer, *J. Am. Chem. Soc.*, 2010, **132**(24), 8230–8231.

19 W. Cao, S. Xia, M. Appold, N. Saxena, L. Bießmann, S. Grott, N. Li, M. Gallei, S. Bernstorff and P. Müller-Buschbaum, *Sci. Rep.*, 2019, **9**(1), 18269.

20 J. M. Widin, A. K. Schmitt, K. Im, A. L. Schmitt and M. K. Mahanthappa, *Macromolecules*, 2010, **43**(19), 7913–7915.

21 J. M. Widin, A. K. Schmitt, A. L. Schmitt, K. Im and M. K. Mahanthappa, *J. Am. Chem. Soc.*, 2012, **134**(8), 3834–3844.

22 A. K. Schmitt and M. K. Mahanthappa, *Macromolecules*, 2017, **50**(17), 6779–6787.

23 C. S. Sample, E. A. Kellstedt and M. A. Hillmyer, *ACS Macro Lett.*, 2022, **11**(5), 608–614.

24 L. M. Pitet and M. A. Hillmyer, *Macromolecules*, 2009, **42**(11), 3674–3680.

25 C. De Rosa, A. Malafronte, R. Di Girolamo, F. Auriemma, M. Scoti, O. Ruiz de Ballesteros and G. W. Coates, *Macromolecules*, 2020, **53**(22), 10234–10244.

26 T. R. Panthani and F. S. Bates, *Macromolecules*, 2015, **48**(13), 4529–4540.

27 W. Limsukon, R. Auras and T. Smith, *ACS Appl. Polym. Mater.*, 2021, **3**(11), 5920–5931.

28 A. Al-Jumaili, S. Alancherry, D. Grant, A. Kumar, K. Bazaka and M. V. Jacob, *Non-thermal plasma technology for polymeric materials*, 2019, pp. 211–240.

29 S. B. Hong, S. J. Hong, T.-H. Kang, J. H. Youk and W.-R. Yu, *J. Polym. Sci., Part B: Polym. Phys.*, 2017, **55**(21), 1595–1607.

30 M. Van der Walt, T. Crabtree and C. Albantow, *Australas. Phys. Eng. Sci. Med.*, 2019, **42**(4), 1165–1176.

31 S. Farah, D. G. Anderson and R. Langer, *Adv. Drug Delivery Rev.*, 2016, **107**, 367–392.

32 T. Vidil, N. Hampu and M. A. Hillmyer, *ACS Cent. Sci.*, 2017, **3**(10), 1114–1120.

33 J. R. Dorgan, J. Janzen, D. M. Knauss, S. B. Hait, B. R. Limoges and M. H. Hutchinson, *J. Polym. Sci., Part B: Polym. Phys.*, 2005, **43**(42), 3100–3111.

34 W. A. Schneider and M. F. Müller, *J. Mol. Catal.*, 1988, **46**(1–3), 395–403.

35 A. S. Zalusky, R. Olayo-Valles, J. H. Wolf and M. A. Hillmyer, *J. Am. Chem. Soc.*, 2002, **124**(43), 12761–12773.

36 K. S. Anderson, S. H. Lim and M. A. Hillmyer, *J. Appl. Polym. Sci.*, 2003, **89**(14), 3757–3768.

37 X. Liang, X. Zhang, L. Zhang, L. Liu, J. Du, X. Zhu and K. M. Ng, *Ind. Eng. Chem. Res.*, 2019, **58**(34), 15542–15552.

38 L. M. Pitet, B. M. Chamberlain, A. W. Hauser and M. A. Hillmyer, *Polym. Chem.*, 2019, **10**(39), 5385–5395.

39 M. W. Matsen and F. S. Bates, *Macromolecules*, 1996, **29**(4), 1091–1098.

40 S. Xi, *et al.*, *Ind. Eng. Chem. Res.*, 2023, **62**(40), 16447–16455.

41 B. Fayolle, *et al.*, *Polym. Degrad. Stab.*, 2000, **70**(3), 333–340.

42 G. Levitin, K. Reinhardt and D. Hess, *Plasma cleaning for electronic, photonic, biological, and archeological applications*, 2012, ch. 2, pp. 55–106.

43 S. Subrahmanyan, An investigation of pore collapse in asymmetric polysulfone membranes, 2003 (Doctoral dissertation, Virginia Tech).

44 B. Jaleh, P. Parvin, P. Wanichapichart, A. P. Saffar and A. Reyhani, *Appl. Surf. Sci.*, 2010, **257**(5), 1655–1659.

45 H. Y. Yu, X. C. He, L. Q. Liu, J. S. Gu and X. W. Wei, *Plasma Processes Polym.*, 2008, **5**(1), 84–91.

46 J. Wang, *et al.*, *Membranes*, 2018, **8**(3), 56.

47 K. Sing, *Colloids Surf., A*, 2001, **187**, 3–9.

48 M. Thommes, *Chem. Ing. Tech.*, 2010, **82**(7), 1059–1073.

49 R. Reis, L. F. Dumée, B. L. Tardy, R. Dagastine, J. D. Orbell, J. A. Schutz and M. C. Duke, *Sci. Rep.*, 2016, **6**(1), 29206.

50 G. Primc and M. Mozetič, *Polymers*, 2022, **14**(12), 2496.

51 F. V. Frieß, Q. Hu, J. Mayer, L. Gemmer, V. Presser, B. N. Balzer and M. Gallei, *Macromol. Rapid Commun.*, 2022, **43**(3), 2100632.

52 M. Kukizaki and M. Goto, *J. Memb. Sci.*, 2006, **281**(1–2), 386–396.

53 A. K. A. Ahmed, *et al.*, *Chemosphere*, 2018, **203**, 327–335.

54 M. Kukizaki and T. Wada, *Colloids Surf., A*, 2008, **317**(1–3), 146–154.

55 R. J. Chethalen, E. J. Fastow, E. B. Coughlin and K. I. Winey, *ACS Macro Lett.*, 2023, **12**(1), 107–112.